Polymer Journal
https://doi.org/10.1038/s41428-026-01145-w

ORIGINAL ARTICLE

Dimensional characterization of isolated ethylcellulose in tetrahydrofuran

Kenji Fukuda[1,2] · Moriya Kikuchi[3] · Seigou Kawaguchi[1]

Received: 17 November 2025 / Revised: 29 December 2025 / Accepted: 4 January 2026
© The Author(s) 2026. This article is published with open access

Abstract

The dimensional characterization of ethylcellulose (cellulose ethyl ether, EC_x, where x is the degree of substitution based on the number of hydroxyl groups in a repeating unit (in this study, $x = 3.0$ and 2.5)) with a weight-averaged molar mass (M_w) ranging from 6.32×10^3 to 3.83×10^5 g mol^{-1} and a relatively narrow molar mass distribution ($M_w/M_n < 1.2$) was studied in tetrahydrofuran (THF) at 25 °C using static light and small-angle X-ray scattering and intrinsic viscosity ([η]) measurements. Eleven fully substituted $EC_{3.0}$ samples with M_w/M_n values ranging from 1.05 to 1.22 were prepared by reacting commercially available $EC_{2.5}$ with ethyl iodide in THF at 55 °C in the presence of sodium hydride, followed by fractionation using recycling preparative size exclusion chromatography (SEC) in $CHCl_3$. Furthermore, eight $EC_{2.5}$ samples with M_w/M_n values ranging from 1.04 to 1.19 were obtained by applying the same fractionation technique to $EC_{2.5}$. Afterward, the z-averaged root-mean-squared radius of gyration ($< S^2 >_z^{1/2}$) and [η] for the isolated $EC_{3.0}$ and $EC_{2.5}$ chains were measured and tabulated as functions of M_w. Furthermore, their M_w dependencies were analyzed using cylindrical wormlike chain and wormlike touched-bead models. The chain stiffness parameter (Kuhn segment length, λ^{-1}), molar mass per unit contour length (M_L), and hydrodynamic bead diameter (d_B) were determined to be 23.1 nm, 491 g mol^{-1} nm^{-1}, and 1.8 nm for $EC_{3.0}$ and 16.5 nm, 467 g mol^{-1} nm^{-1}, and 1.1 nm for $EC_{2.5}$, respectively. These results indicate that both $EC_{3.0}$ and $EC_{2.5}$ form semiflexible chains with moderate stiffness, primarily because of steric hindrance arising from the ethyl groups in the cellulose backbone. The monomer counter length (l_M) was estimated to be 0.50 nm for both $EC_{3.0}$ and $EC_{2.5}$, suggesting that the local conformation of the EC chain remains largely unaffected by x between 2.5 and 3.0. In addition, the l_M value was almost equal to that (0.51–0.52 nm) of crystalline cellulose but considerably greater than that (0.33 nm) of α-1,4-linked amylose derivatives. In contrast, λ^{-1} and d_B were influenced by x, likely because of greater steric hindrance in the main chain and desolvation around the hydroxyl groups.

Introduction

Cellulose derivatives are biobased polymers in which some or all the hydroxyl groups are replaced with other functional groups; thus, their solubility in solvents and thermal properties can be controlled to suit various applications [1]. Modification of the hydroxyl groups can yield cellulose ethers or esters, depending on the substituent [1]. Ethylcellulose (denoted EC_x, where x is the degree of substitution based on the number of hydroxyl groups in a repeating unit and varies from 0 to 3) is a cellulose ether (Fig. 1) prepared by substituting ethoxy groups at the hydroxyl positions. For $x = 0.8$–1.7, EC is soluble in water, whereas for $x > 1.7$, it dissolves only in organic solvents [1].

EC_x has broad applications, for example, in cosmetics and as adhesives, binders, coating agents, thickeners, film-forming agents, plasticizers, and excipients [1].

Supplementary information The online version contains supplementary material available at https://doi.org/10.1038/s41428-026-01145-w.

✉ Moriya Kikuchi
m-kikuchi@yz.yamagata-u.ac.jp

✉ Seigou Kawaguchi
skawagu@yz.yamagata-u.ac.jp

[1] Department of Organic Materials Science, Graduate School of Organic Materials Science, Yamagata University, Yonezawa, Japan

[2] Sumitomo Metal Mining Co. Ltd., Minato-ku, Japan

[3] Faculty of Engineering, Yamagata University, Yonezawa, Japan

Published online: 13 February 2026

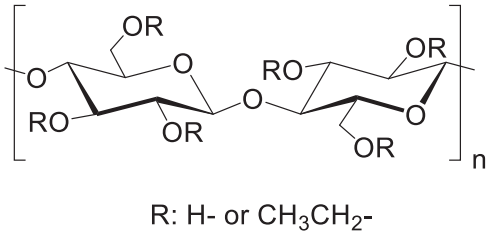

Fig. 1 Chemical structure of EC_x ($x = 3.0$ and 2.5)

Furthermore, owing to its solubility in organic solvents, it is used in pharmaceuticals, inks, paints, adhesives, plastics, textile finishing agents, and electronic materials [1]. Most commercial ECs have $x = 2.5$ and thus dissolve in various organic solvents. $EC_{2.5}$ is frequently used as a rheology control agent and binder for inorganic particle dispersions [2–12]; a primary application is the preparation of nickel paste for multilayer ceramic capacitors (MLCCs), which are essential electronic components in modern society. The main component consists of submicron-sized nickel particles (50 wt%) and barium titanate particles (5–15 wt%), the latter serving as a sintering inhibitor. The paste also contains binder resins, $EC_{2.5}$, solvents such as α-terpineol and dihydroterpineol, and additives, including dispersants and plasticizers [4, 11]. Recently, demand has increased for smaller nickel particles, which enhance performance (e.g., increased capacitance) and enable the miniaturization of MLCCs. However, as the particle size decreases, the rheological properties of the paste change significantly [11]. Furthermore, the effects of each component, as well as the mechanisms underlying these effects, remain unclear, making it challenging to design a nickel paste that meets all the requirements.

A key material governing the rheological properties of the nickel paste is $EC_{2.5}$. It has been reported that a transient network structure forms in the paste through the cross-linking (bridging) of particles by $EC_{2.5}$ molecules [2, 3]. However, the mechanism by which $EC_{2.5}$ and the particles interact to form a network structure remains unclear. $EC_{2.5}$ has also been reported to aggregate in solvents such as α-terpineol and other organic solvents [13], suggesting that this may be the mechanism underlying network formation (note that the network is also loosened by shearing). Given that the internal structure of nickel paste is poorly understood, nickel-paste-based products are developed through trial and error. Therefore, understanding the conformational properties of isolated $EC_{2.5}$ chains in solvents and determining the molecular parameters characteristic of $EC_{2.5}$ would aid in elucidating its effects on rheological properties, including the state of nickel paste under shear and aggregate dissociation, and contribute to the design of next-generation nickel pastes.

To date, there have been few reports on the molecular characterization of isolated $EC_{2.5}$ chains in solution. For example, Moore and Brown [14] and Scherer et al.[15] reported the dilute solution properties of $EC_{2.5}$ with molar masses ranging from 1×10^4 to 2×10^5 g mol^{-1}, as determined by viscosity measurements in ethyl acetate and chloroform. Meyerhoff and Sütterlin [16] also reported the dilute solution properties of $EC_{2.7}$ with molar masses ranging from 1×10^4 to 1.4×10^5 g mol^{-1}, as determined by light-scattering measurements in ethyl acetate. Furthermore, Hua et al.[13] demonstrated that $EC_{2.5}$ molecules aggregate in dilute organic solvents, yielding nearly monodisperse 200–300-nm-sized colloidal particles without isolated chains. However, because significant heterogeneity in molar mass ($M_w/M_n > 2.3$, where M_w and M_n are the weight- and number-averaged molar masses, respectively) and x in the samples was not fully considered, the molecular characterization of isolated $EC_{2.5}$ chains in solution remains incomplete. Furthermore, the effect of x on the molecular conformation of the EC chain remains poorly understood.

In this study, we focused on fully substituted EC ($EC_{3.0}$) with a uniform degree of substitution to eliminate ambiguity and determined its conformational properties in tetrahydrofuran (THF) at 25 °C. The $EC_{3.0}$ sample was prepared by reacting commercially available $EC_{2.5}$ with ethyl iodide at 55 °C in the presence of sodium hydride. The synthesized $EC_{3.0}$ sample was further fractionated by recycling preparative size exclusion chromatography (SEC) into 11 components with narrow molar mass distributions ($M_w/M_n < 1.22$) and a molar mass range of 7.05×10^3 to 1.87×10^5 g mol^{-1}. These samples were analyzed by SEC fitted with a multiangle light scattering (MALS) detector and a viscosity (Vis) detector in THF at 25 °C. Additionally, small-angle X-ray scattering (SAXS) measurements were conducted on the lower-molar-mass sample. The z-averaged root-mean-squared radius of gyration ($<S^2>_z^{1/2}$) and intrinsic viscosity ([η]) of $EC_{3.0}$ were measured and rationalized as functions of M_w. Furthermore, the experimental data were analyzed using cylindrical wormlike chain and wormlike touched-bead models to determine the molecular parameters characteristic of the $EC_{3.0}$ chain. In addition, similar fractionation, measurements, and analyses were performed on $EC_{2.5}$, and the molecular conformational properties of an isolated $EC_{2.5}$ chain in THF were clarified by comparison with those of $EC_{3.0}$.

Experimental section

Materials

Three $EC_{2.5}$ samples (STD-4, 45, and 300) were purchased from Dow Chemical Co., USA, and used after they were vacuum dried at 60 °C for more than 24 h. THF (> 99.5%) was used as the solvent and was purchased from Kanto

Table 1 Molecular characteristics of $EC_{3.0}$ in THF at 25 °C, determined by SEC–MALS–Vis measurements

Sample	$M_w \times 10^{-5}$ (g mol^{-1})		M_w/M_n		$M_w \times 10^{-5}$ [c] (g mol^{-1})	M_w/M_n [c]	RV_p [d] (cm^3)	$M_w \times 10^{-5}$ [f] (g mol^{-1})	$<S^2>_z^{1/2}$ [h] (nm)	$[\eta]$ [k] (g^{-1} cm^3)
	(PS)[a]	($EC_{3.0}$)[b]	(PS)[a]	($EC_{3.0}$)[b]						
$EC_{3.0}$−1	0.135	0.0705	1.26	1.16	0.0736	1.01	28.23	0.0800	3.9[j]	27.2
$EC_{3.0}$−2	0.246	0.116	1.08	1.05	0.116	1.03	27.53	0.112	5.7[j]	41.0
$EC_{3.0}$−3	0.382	0.168	1.09	1.06	0.158	1.02	26.92	0.156	7.5	56.0
$EC_{3.0}$−4	0.398	0.174	1.09	1.07	0.174	1.03	26.77	0.174	8.2	62.8
$EC_{3.0}$−5	0.727	0.288	1.14	1.10	0.276	1.05	26.07	0.247	10.3	92.6
$EC_{3.0}$−6	0.911	0.346	1.21	1.15	0.352	1.07	25.71	0.305	12.4	118
$EC_{3.0}$−7	1.63	0.570	1.08	1.06	0.555	1.02	24.51	0.545	17.4	212
$EC_{3.0}$−8	2.39	0.822	1.15	1.13	0.788	1.05	23.92	0.759	21.9	299
$EC_{3.0}$−9	3.07	1.06	1.22	1.22	0.937	1.08	23.68	0.872	24.0	313
$EC_{3.0}$−10	4.21	1.47	1.19	1.19	1.38	1.08	23.00	1.28	29.9	440
							22.47	1.91	38.8	680
$EC_{3.0}$−11	5.33	1.87	1.19	1.20	1.94	1.13	22.17[e]	2.22[g]	42.2[i]	767[l]
							21.87[e]	2.68[g]	45.3[i]	915[l]

[a]Determined from the PS calibration curve

[b]Determined from the absolute calibration curve of $EC_{3.0}$ (Fig. 2(a))

[c]Determined by SEC-MALS

[d]RV_p is the RV at the peak top in a RI chromatogram

[e]RV other than RV_p

[f]M_w at RVp

[g]M_w at the indicated RV

[h]$<S^2>_z^{1/2}$ at RV_p

[i]$<S^2>_z^{1/2}$ at the indicated RV

[j] Determined by SAXS in THF at 25 °C

[k]$[\eta]$ at RV_p

[l]$[\eta]$ at the indicated RV

Kagaku Co., Ltd., Tokyo, Japan, and distilled over sodium. Ethyl iodide and chloroform-d (99.8%) were purchased from Kanto Kagaku Co., Ltd., Tokyo, Japan, and used without further purification. Chloroform (99.0%, Junsei Chemical Co., Ltd., Tokyo, Japan) was used as received. Spectroscopic-grade THF, which was used for SAXS, differential refractive index increment, and partial specific volume measurements, was purchased from Kanto Kagaku Co., Ltd., Tokyo, Japan, and used as received.

The ethylation of $EC_{2.5}$ (STD-4, 45, and 300) was performed according to the method reported by Budgell [17]. Briefly, the reaction was carried out in THF at 55 °C for 5 h, using eight equivalents of ethyl iodide relative to the remaining hydroxyl groups, in the presence of sodium hydride under a nitrogen atmosphere. The reaction mixture was reprecipitated in deionized water, centrifuged, and vacuum-dried. The dried sample was redissolved in THF, reprecipitated, centrifuged, vacuum-dried, and subsequently redissolved as described above. This process was repeated five times for purification. In the first and second precipitation steps, sodium thiosulfate was added to deionized water at a 2:1000 weight ratio to prevent the formation of free iodine. By modifying $EC_{2.5}$, fully ethylated $EC_{3.0}$ samples were prepared with 0.13×10^4 g mol^{-1} < M_n < 5.3×10^4 g mol^{-1} relative to a polystyrene (PS) SEC calibration. These samples were further fractionated using recycling preparative SEC (NEXT, Japan Analytical Industry (JAI) Co., Ltd., Japan) at 22–26 °C. The experimental conditions were as follows: chloroform eluent, 7–14 cm^3 min^{-1} flow rate, 3H-40 and 4H-40 (JAI Co., Ltd., Japan) columns, 5–10 cm^3 injection volume, and 1–5 wt% concentration. Finally, eleven $EC_{3.0}$ samples with $M_w/M_n < 1.22$ and M_w values ranging from 7.05×10^3 to 1.87×10^5 g mol^{-1} were prepared (Table 1). The fractionation of unmodified $EC_{2.5}$ (STD-4, 45, and 300) was also conducted in the same manner, and eight $EC_{2.5}$ samples with $M_w/M_n < 1.19$ and M_w values ranging from 6.32×10^3 to 2.50×10^5 g mol^{-1} were collected (Table 2).

Measurements

^{1}H NMR measurements were carried out in chloroform-d using a JEOL JNM-ECX 400 MHz apparatus; the degree of substitution (x) was estimated as $x = 3(7b/(9a–6b))$, in which b is the integrated intensity of the signal from CH_3 in

Table 2 Molecular characteristics of $EC_{2.5}$ in THF at 25 °C, determined by SEC-MALS-Vis measurements

Sample	x[a]	$M_w \times 10^{-5}$ (g mol^{-1})		M_w/M_n		$M_w \times 10^{-5}$ [d] (g mol^{-1}	M_w/M_n[d]	RV_p[e] (cm^3)	$M_w \times 10^{-5}$ [g] (g mol^{-1})	$\langle S^2 \rangle_z^{1/2}$ [i] (nm)	$[\eta]$ [l] (g^{-1} cm^3)
		(PS)[b]	($EC_{2.5}$)[c]	(PS)[b]	($EC_{2.5}$)[c]						
$EC_{2.5}$-1	2.59	0.0944	0.0632	1.07	1.04	0.0657	1.03	29.00	0.0634	3.3[k]	15.2
$EC_{2.5}$-2	2.48	0.166	0.0994	1.09	1.06	0.0953	1.04	28.12	0.0994	4.9[k]	25.8
$EC_{2.5}$-3	2.48	0.349	0.190	1.20	1.14	0.185	1.08	27.05	0.184	7.9	49.6
$EC_{2.5}$-4	2.62	0.605	0.302	1.13	1.09	0.302	1.04	26.03	0.311	11.3	87.0
$EC_{2.5}$-5	2.55	1.18	0.517	1.24	1.16	0.523	1.08	25.01	0.529	15.8	135
$EC_{2.5}$-6	2.60	1.57	0.662	1.22	1.16	0.627	1.11	24.75	0.565	16.6	167
								23.77	0.973	22.8	263
$EC_{2.5}$-7	2.43	2.87	1.15	1.21	1.19	1.11	1.14				
								23.16[f]	1.29[h]	26.9[j]	349[m]
								22.47	2.20	36.4	460
								22.17[f]	2.58[h]	39.1[j]	564[m]
$EC_{2.5}$-8	2.59	6.13	2.50	1.17	1.19	2.53	1.11				
								21.87[f]	3.07[h]	43.0[j]	680[m]
								21.57[f]	3.83[h]	47.6[j]	812[m]

[a]The degree of substitution, determined by ^{1}H NMR (Fig. S1)

[b]Determined by the PS calibration curve

[c]Determined from the absolute calibration curve of $EC_{2.5}$ (Fig. 2(b))

[d]Determined by SEC-MALS

[e]RV_p is the RV at the peak top in a RI chromatogram

[f]RV other than RV_p. [g]M_w at RV_p. [h]M_w at the indicated RV

[i]$\langle S^2 \rangle_z^{1/2}$ at RV_p. [j]$\langle S^2 \rangle_z^{1/2}$ at the indicated RV

[k]Determined by SAXS in THF at 25

[m]$[\eta]$ at the indicated RV

the ethyl groups and a is that from CH and CH_2 in the glucose unit and ethyl group (Fig. S1). The partial specific volume (v_{sp}) of the $EC_{3.0}$-6 and $EC_{2.5}$-4 samples in THF was measured at 25 °C using a DMA 4500 M densimeter (Anton Paar GmbH, Austria) as the EC mass concentration C (g cm^{-3}) was varied from 4.0 to 10.0 mg cm^{-3}. The differential refractive index increments (dn/dc) for $EC_{3.0}$-6 and $EC_{2.5}$-3 were determined in THF at 25 °C using a differential refractometer (Otsuka Electronics DRM-1021, wavelength $\lambda = 632.8$ nm) as C was varied from 2.5 to 6.0 mg cm^{-3}.

The M_w, $\langle S^2 \rangle_z^{1/2}$, and $[\eta]$ for a series of $EC_{3.0}$ and $EC_{2.5}$ samples were measured by SEC fitted with a MALS detector (Wyatt Technology Corporation DAWN HELEOS, $\lambda = 658$ nm), a refractive index detector (RI: Wyatt Technology Corporation Optilab T-rEX, $\lambda = 658$ nm), and a viscometer (Vis; Viscotek Technology Co. T-60A Dual Detector) at 25 °C. The SEC measurements were carried out at a column temperature of 25 °C using THF as the eluent at a flow rate of 1.0 cm^3 min^{-1}, with a DG-2080-53 degasser (Jasco Corp.), a 1100 Series isocratic pump (Agilent Corp.), a CO-2060 Plus column oven (Jasco Corp.), and three Tosoh TSKgel GMHHR-H (S) columns.

Notably, $EC_{2.5}$ aggregates in most organic solvents [13], thereby making studies of isolated chains extremely difficult. Through trial and error, we discovered that isolated $EC_{2.5}$ chains can be studied using the following solution preparation method. All sample solutions for v_{sp}, dn/dc, SAXS, and SEC-MALS-Vis measurements were prepared by dissolving $EC_{3.0}$ and $EC_{2.5}$ in THF at 50 °C, and the temperature was maintained at 50 °C until immediately before measurement. The calibration of the MALS and Vis devices and the MALS analysis were performed according to previously reported methods [18, 19].

With respect to the SEC-MALS measurements, SEC column cleaning is crucial. Many commercially available columns contain impurities within their micro- and nano-pores, resulting in a low signal-to-noise ratio in light-scattering intensities, even when the RI and MALS signals are stable enough for the measurements. Thus, thorough column cleaning is required to achieve accurate determinations of the molar mass and radius of gyration, particularly for polymers with low M_w and dn/dc values [20]. Furthermore, the delay volume between the RI and MALS detectors can be determined accurately using the new method we have developed [20]. By considering these

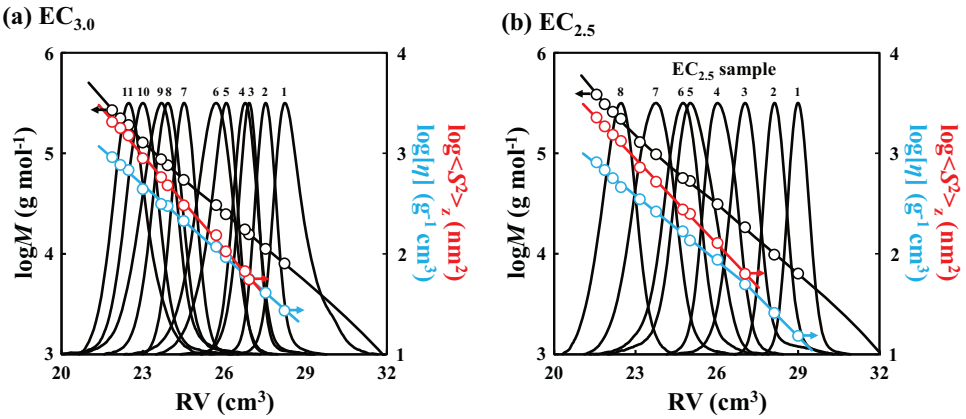

Fig. 2 SEC chromatograms of the **a** $EC_{3.0}$ (left) and **b** $EC_{2.5}$ (right) samples used in this study; the M_w, $<S^2>_z$, and $[\eta]$ determined by SEC-MALS-Vis are also shown

points, it is possible to reliably evaluate the molar mass and molar mass distribution using SEC-MALS.

SAXS measurements were performed in THF at 25 °C on a NANO-Viewer (Rigaku Co.) with a Pilatus 100 K detector (DECTRIS Co.), an X-ray wavelength (λ) of 0.15418 nm, and a camera length of 630 mm [19]. The scattering vector (q) is defined as $q = 4\pi\sin\theta/\lambda$ at the scattering angle (2θ). The excess scattering intensity $[\Delta I(q)]$ was obtained from the scattering intensity difference corrected by the X-ray transmittance for the solution and solvent at the same q. SAXS measurements were carried out at four different concentrations, and $[C/\Delta I(q)]^{1/2}$ was plotted against C, yielding $[C/\Delta I(q)]^{1/2}_{C\to 0}$ at infinite dilution by extrapolating the data points at each q to zero concentration using least squares [21]. Notably, when $EC_{2.5}$ was dissolved in THF at room temperature, significant scattering was observed in the low-q region, which was attributed to aggregate formation. However, after dissolving $EC_{2.5}$ in THF at 50 °C and maintaining it at that temperature until immediately before measurement, this aggregate scattering completely disappeared within at least 1.5 h, and normal scattering profiles from isolated $EC_{2.5}$ chains were obtained.

Results and discussion

Fully ethylated $EC_{3.0}$ with $x = 3.0$ was prepared, as confirmed by ^{1}H-NMR measurements (Fig. S1). Figure 2 shows the SEC traces (THF as the eluent) of the eleven $EC_{3.0}$ and eight $EC_{2.5}$ samples fractioned by recycling preparative SEC using $CHCl_3$ as the eluent. The M_w, $<S^2>_z^{1/2}$, and $[\eta]$, determined from the SEC-MALS-Vis measurements, are also plotted against the retention volume (RV). The M_w, $<S^2>_z^{1/2}$, and $[\eta]$ reasonably decrease as the RV increases, indicating that the SEC separation conditions are appropriate for $EC_{3.0}$ and $EC_{2.5}$. Crucially, our solution preparation method enables measurements of isolated $EC_{2.5}$ chains. The M_w and M_w/M_n values for $EC_{3.0}$ and $EC_{2.5}$, averaged over the entire eluted substance, were estimated from the absolute calibration curves constructed with $EC_{3.0}$ and $EC_{2.5}$ as standards, along with ethylbenzene (not shown). These values are listed in Tables 1 and 2, along with those obtained from the conventional calibration curve using PS standards, for comparison. The apparent M_w values from the PS calibration curve are approximately two- to threefold greater because of the differences in the molecular structure of the repeating unit and the conformation between PS and EC. The M_w/M_n values determined from the PS calibration are also higher than those from the absolute calibration, implying that the $EC_{3.0}$ and $EC_{2.5}$ chains are considerably stiffer than the flexible PS chains. The M_w and M_w/M_n values determined by SEC-MALS are also listed in Tables 1 and 2, and the M_w values are very close to those determined by absolute calibration within experimental error. In contrast, the M_w/M_n values obtained by SEC-MALS are significantly lower than those obtained by absolute calibration, likely because of band broadening in the latter method [20]. Considering that SEC-MALS measurements for polymers with narrow molar mass distributions may contain errors in the high-RV region of the chromatogram, resulting in an underestimation of M_w/M_n [20], the actual M_w/M_n value may lie between the two values. Since the M_w, $<S^2>_z^{1/2}$, and $[\eta]$ values at the peak top of the RI signal (RV_p) in the SEC-MALS-Vis chromatogram are most reliable, they were used to study the following dimensional properties (Tables 1 and 2). For the high-molar-mass samples $EC_{3.0}$-11, $EC_{2.5}$-7, and $EC_{2.5}$-8, the highly reliable values for components eluted before RV_p were also used. When using $<S^2>_z^{1/2}$ obtained from SAXS measurements, the M_w value derived from the absolute calibration curve was employed.

First, the partial specific volume (v_{sp}), which may be related to the conformational properties, state (aggregated or not), and polymer–solvent interactions, is described. Figure 3(a) shows the plots of $(\rho_s - \rho_0)$ versus C for $EC_{3.0}$-6 and $EC_{2.5}$-4 in THF at 25 °C. Here, v_{sp} was determined using Eq. 1.

$$\rho_s = \rho_0 + (1 - v_{sp}\rho_0)C \quad (1)$$

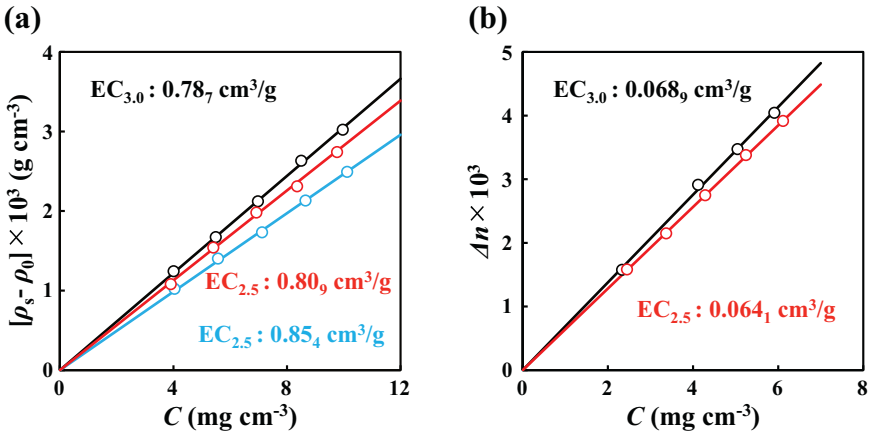

Fig. 3 **a** Plots of $[\rho - \rho_0]$ versus C for $EC_{3.0}$-6 and $EC_{2.5}$-4 in THF at 25 °C. Data (blue circles) for the $EC_{2.5}$−4 solution prepared at 25 °C are also shown. **b** Plots of Δn vs. C for $EC_{3.0}$-6 and $EC_{2.5}$−4 in THF at 25 °C

Table 3 dn/dc, v_{sp}, and the cylindrical wormlike chain and wormlike touched-bead model parameters characteristic of isolated $EC_{3.0}$ and $EC_{2.5}$ chains in THF at 25 °C

Polymer	M_0 (g mol^{-1})	dn/dc (cm^3 g^{-1})	v_{sp} (cm^3 g^{-1})	M_L (g mol^{-1} nm^{-1})	l_M (nm)	λ^{-1} (nm)	$\langle S_c^2 \rangle^{1/2}$ [a] (nm)	d_B (nm)	λB
$EC_{3.0}$	246.3	0.068_9	0.78_7	491	0.50_2	23.1	0.21	1.8	0.10
$EC_{2.5}$	231.8	0.064_1	0.80_9	467	0.49_6	16.5	0.21	1.1	0.05

[a]Determined by SAXS

Here, ρ_0 and ρ_s are the densities of the solvent and solution, respectively. The v_{sp} values determined from the slope and ρ_0 are listed in Table 3. Almost identical values of 0.787 and 0.809 cm^3 g^{-1} for $EC_{3.0}$ and $EC_{2.5}$, respectively, are obtained; these values are smaller than that (0.905 cm^3 g^{-1}) of flexible PS in THF [22] and that (0.95 cm^3 g^{-1}) of semiflexible poly(*n*-hexyl isocyanate) in hexane [23] and slightly larger than that (0.714–0.724 cm^3 g^{-1}) of amylose *tris*(phenylcarbamate) in 1,4-dioxane at 25 °C [24]. Measurements were also performed on the THF solution of $EC_{2.5}$ prepared at 25 °C, as indicated by the blue circles in Fig. 3(a). A significantly larger value (0.854 cm^3 g^{-1}) than that for the $EC_{2.5}$ solution prepared at 50 °C is obtained, although it is very close to the range (≈0.84–0.90 cm^3 g^{-1}) reported at 25 °C in various solvents [16]. The difference in v_{sp} arises from differences in sample preparation methods, although both solutions are transparent and homogeneous. It is possible that $EC_{2.5}$ is aggregated at 25 °C, yielding a colloidal dispersion [13]. This aggregate cannot be unraveled in THF at 25 °C. Assuming that the aggregates are rigid bodies and impermeable to the solvent, v_{sp} may be equal to the reciprocal of the solute density. As the density of solid $EC_{2.5}$ is 1.14 cm^3 g^{-1} at 25 °C, v_{sp} is calculated to be 0.877 cm^3 g^{-1}, which is close to the observed and literature values. Therefore, $EC_{3.0}$ molecularly dissolves in THF, regardless of the sample preparation temperature, but $EC_{2.5}$ forms colloidal aggregated particles in THF at 25 °C. Crucially, the $EC_{2.5}$ aggregates in THF dissociate upon heating to 50 °C, enabling the study of the dilute-solution properties of isolated $EC_{2.5}$ chains. Figure 3(b) shows the excess refractive index Δn plotted against C. The dn/dc values were determined from the slopes (Table 3). Slight differences in dn/dc can be interpreted as resulting from differences in the chemical composition with respect to x.

The root plots of $[C/\Delta I(q)]_{C\to 0}^{1/2}$ versus q^2 obtained from SAXS measurements for the $EC_{3.0}$-1, $EC_{3.0}$-2, $EC_{2.5}$-1, and $EC_{2.5}$-2 samples with low M_w in THF at 25 °C are shown in Fig. 4. Normal root plots without any increase in the scattering intensities in the low-q region are observed, indicating the absence of $EC_{2.5}$ aggregates in THF. The experimental profiles show some variation because of the small difference in electron density, but the $\langle S^2 \rangle_z^{1/2}$ value can be determined from the initial slope and intercept of the straight line (solid red lines in Fig. 4) with sufficiently high reliability using Eq. 2, and the results are listed in Table 1 and 2.

$$\left(\frac{C}{\Delta I(q)}\right)_{C\to 0}^{1/2} = \left(\frac{C}{\Delta I(0)}\right)_{C\to 0}^{1/2} + \frac{1}{6}\left(\frac{C}{\Delta I(0)}\right)_{C\to 0}^{1/2} \langle S^2 \rangle_z q^2 + \cdots\cdots \quad (2)$$

Figure 5(a) shows a double logarithmic plot of $\langle S^2 \rangle_z^{1/2}$ versus M_w for $EC_{3.0}$ and $EC_{2.5}$, as obtained by SAXS and SEC-MALS measurements. Figure 5(b) shows the results plotted against the degree of polymerization, N_w, as the molar mass of the repeating unit changes between $EC_{3.0}$ and $EC_{2.5}$. These figures indicate that both $EC_{3.0}$ and $EC_{2.5}$ exhibit the typical M_w- and N_w-dependent behavioral characteristics of semiflexible linear polymers, where in the low-M_w region, the slope is greater than 0.6 but decreases with increasing M_w. The relationships between $\langle S^2 \rangle_z^{1/2}$ and M_w for $EC_{3.0}$ and $EC_{2.5}$ isolated chains in THF at 25 °C are given in Eq. 3.

$$\begin{aligned} &EC_{3.0}: \langle S^2\rangle_z^{\frac{1}{2}}(\mathrm{nm}) = 3.6\times10^{-3}M_w^{0.79}[7.05\times10^3 < M_w < 2.47\times10^4] \quad \langle S^2\rangle_z^{1/2}(\mathrm{nm}) = 2.6\times10^{-2}M_w^{0.60}[3.05\times10^4 < M_w < 2.68\times10^5] \\ &EC_{2.5}: \langle S^2\rangle_z^{1/2}(\mathrm{nm}) = 3.1\times10^{-3}M_w^{0.80}[9.94\times10^3 < M_w < 1.83\times10^4] \quad \langle S^2\rangle_z^{1/2}(\mathrm{nm}) = 3.6\times10^{-2}M_w^{0.56}[5.29\times10^4 < M_w < 3.83\times10^5] \end{aligned} \tag{3}$$

The $\langle S^2\rangle_z^{1/2}$ value of $EC_{2.5}$ is always smaller than that of $EC_{3.0}$, with the corresponding N_w, implying that the chains may be markedly different. In addition, the difference in slope in the high-M_w region suggests that THF is a good solvent for $EC_{3.0}$ but not a very good solvent for $EC_{2.5}$. Considering that $EC_{2.5}$ aggregates in THF at 25 °C [13] and that the slope appears to decrease further with increasing M_w, THF might be close to the θ-solvent. Notably, for $EC_{2.5}$, compositional heterogeneity persists (x ranges from 2.43 to 2.62 in Table 2); thus, the results are subject to some uncertainty. However, a comparison with the $EC_{3.0}$ results and the slight difference in the dn/dc values between them allows the study of the molecular chain conformation of $EC_{2.5}$ with considerable confidence.

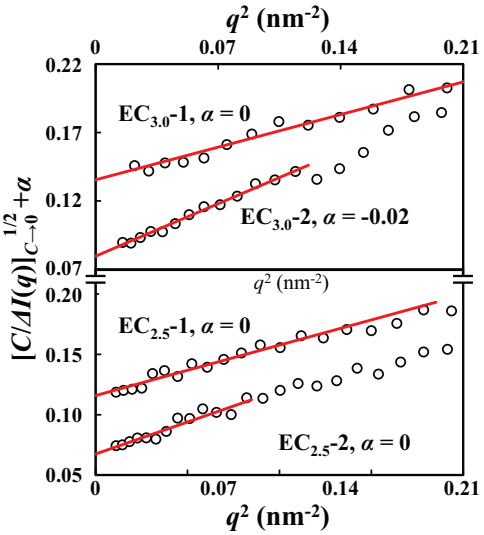

Fig. 4 Root plots of $[C/\triangle I(q)]_{C\to0}^{1/2}$ vs. q^2 for the $EC_{3.0}$ and $EC_{2.5}$ samples in THF at 25 °C. The vertical axis is plotted by adding a factor, α, for clarity. The solid lines show the initial slope within the Guinier region

The molecular parameters characterizing isolated $EC_{3.0}$ and $EC_{2.5}$ chains were evaluated by comparing the experimental data with those obtained using the cylindrical wormlike chain model. The $\langle S^2\rangle$ for an unperturbed wormlike cylinder may be expressed as the sum of the mean-square cross-sectional radius of gyration, $\langle S_c^2\rangle$, and the radius of gyration of the main chain contour, $\langle S_M^2\rangle$ [25]. The value of $\langle S_c^2\rangle$ was first estimated by comparing the experimental and theoretical scattering form factors, $P(q)$. When the Kuhn segment number ($n_K = \lambda L$) is close to 1, the polymer chain is considered a cylinder with contour length L and diameter d, where λ^{-1} is the stiffness parameter, which will be determined later. $P(q)$ for the cylinder is given by Eq. 4 [19].

$$P(q) = 2\int_0^{\pi}\left\{j_0\left[\left(\frac{qL}{2}\right)cos\theta\right]\right\}^2\left\{\frac{J_1\left[\left(\frac{qd}{2}\right)cos\theta\right]}{\left(\frac{qd}{2}\right)cos\theta}\right\}^2 sin\theta d\theta \tag{4}$$

Here, $j_0(x)$ and $J_1(x)$ are the 0th-order spherical and 1st-order Bessel functions, respectively. Figure 6 compares the experimental and theoretical $P(q)$ in a Kratky plot.

The experimental $P(q)$ for $EC_{3.0}$ and $EC_{2.5}$ was quantitatively described using a cylinder with $d = 0.60$ nm, yielding an $\langle S_c^2\rangle^{1/2}$ value of 0.21 nm, assuming the relationship $\langle S_c^2\rangle = (1/8)d^2$. The contribution of $\langle S_c^2\rangle$ to the observed $\langle S^2\rangle_z$ in Tables 1 and 2 is less than 0.1% but was nevertheless considered in the subsequent analysis.

The radius of gyration of the main chain, $\langle S_M^2\rangle = \langle S^2\rangle_z - \langle S_c^2\rangle$, is expressed by the Kratky–Porod (KP) chain ($\langle S^2\rangle_{KP}$) with L and λ^{-1}, as given by Eq. 5 [26].

$$\langle S^2\rangle_{KP} = \frac{L}{6\lambda} - \frac{1}{4\lambda^2} + \frac{1}{4\lambda^3 L} - \frac{1}{8\lambda^4 L^2}[1-\exp(-2\lambda L)] \tag{5}$$

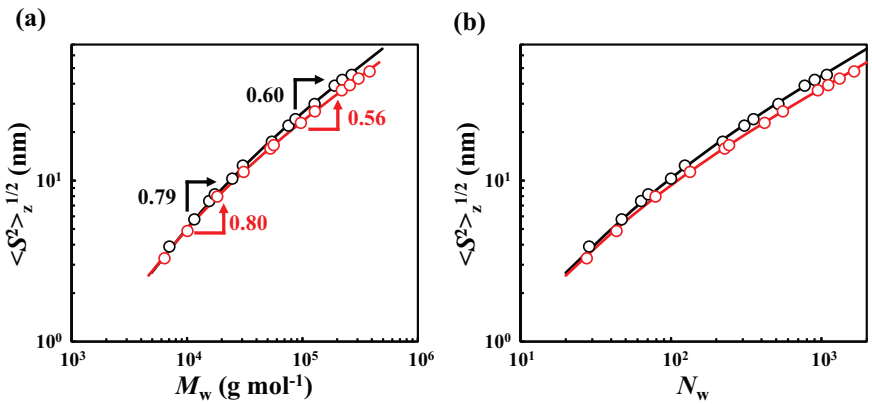

Fig. 5 **a** M_w dependence of $\langle S^2\rangle_z^{1/2}$ for $EC_{3.0}$ and $EC_{2.5}$ in THF at 25 °C and **b** their N_w dependencies. The solid lines represent the theoretical curves for the perturbed cylindrical wormlike chain model using the parameters in Table 3

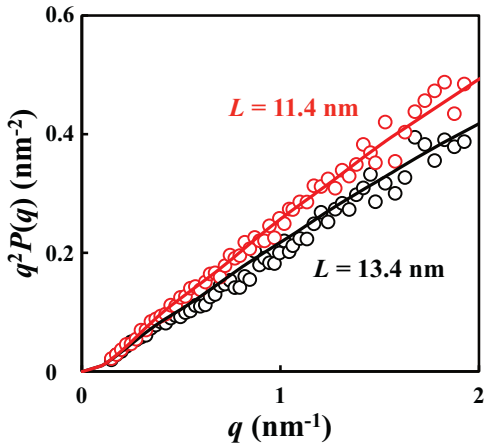

Fig. 6 Kratky plot for $EC_{3.0}$-1 (black circles) and $EC_{2.5}$-1 (red circles) in THF at 25 °C. The black and red curves are the theoretical values calculated from the cylinder model with $d = 0.60$ nm and the indicated L values

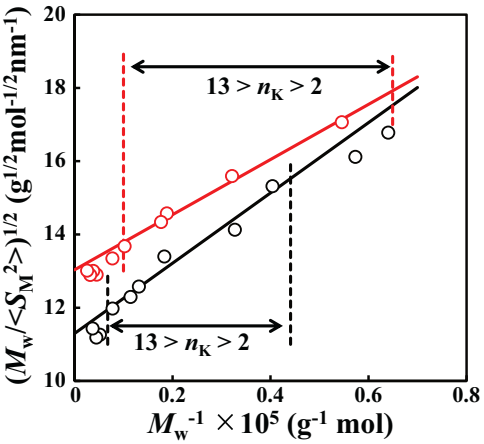

Fig. 7 Plots of $[M_w/\langle S_M^2\rangle]^{1/2}$ vs. $_{Mw}{}^{-1}$ for $EC_{3.0}$ (black circles)) and $EC_{2.5}$ (red circles). The solid lines represent linear regions

L is related to the molecular structure of the polymer according to Eq. 6.

$$L = \frac{M}{M_L} \tag{6}$$

Here, M is the molar mass of the polymer, and M_L is the molar mass per unit contour length. Equation 5 can be approximated as Eq. 7 [27].

$$\left(\frac{M}{\langle S_M^2\rangle}\right)^{1/2} = (6\lambda M_L)^{1/2}\left[1 + \frac{3M_L}{4\lambda}\frac{1}{M}\right] \tag{7}$$

Here, the maximum error from the exact value is 1.5% for $n_K > 2$. The plots of $(M_w/\langle S_M^2\rangle)^{1/2}$ against M_w^{-1} for $EC_{3.0}$ and $EC_{2.5}$ are shown in Fig. 7. As indicated, the linear relationship holds in the region $13 > n_K > 2$. Two molecular parameters characterizing the isolated EC chains, λ^{-1} and M_L, can be estimated from the intercept and slope of the straight line: 23.1 nm and 491 g mol^{-1} nm^{-1} for $EC_{3.0}$ and 16.5 nm and 467 g mol^{-1} nm^{-1} for $EC_{2.5}$, respectively (Table 3).

In the high-M_w region shown in Fig. 7, a downward deviation of the experimental values from the straight line is observed. The deviation is due to excluded-volume effects, which were accounted for using the radius expansion factor (α_S) based on the quasi-two-parameter (QTP) theory [28–31], as given by Eqs. S1–S4 in the SI. The solid lines in Fig. 5(a), (b) show the theoretical curves calculated from the perturbed cylindrical wormlike chain model using the parameters listed in Table 3, where B is the excluded-volume strength and is estimated to be 2.3 nm for $EC_{3.0}$ and 0.83 nm for $EC_{2.5}$ in THF at 25 °C. The significant change in the B value with increasing x is likely due to the polar hydroxyl groups present in $EC_{2.5}$, which substantially increase the intra- and intermolecular attractive interactions between the segments in THF. As shown in Fig. 5, the wormlike chain model quantitatively describes the experimental M_w dependence of $\langle S^2\rangle_z^{1/2}$ for $EC_{3.0}$ and $EC_{2.5}$ over the entire M_w range.

The double logarithmic plots of $[\eta]$ with respect to M_w (a) and N_w (b) for $EC_{3.0}$ and $EC_{2.5}$ in THF at 25 °C are shown in Fig. 8. The M_w dependence of $[\eta]$ for $EC_{3.0}$ and $EC_{2.5}$ shows typical semiflexible polymer behavior, with a power law exponent greater than 0.8. In addition, the $[\eta]$ value for $EC_{3.0}$ is always greater than that for $EC_{2.5}$ at the same N_w, as in the N_w dependence of $\langle S^2\rangle_z^{1/2}$. The Mark–Houwink–Sakurada equations are given in Eq. 8.

$$\begin{aligned} EC_{3.0}: \quad & [\eta](cm^3/g) = 1.7\times10^{-3}M_w{}^{1.08}\ [8.00\times10^3 < M_w < 3.05\times10^4] \quad [\eta](cm^3/g) = 9.6\times10^{-3}M_w{}^{0.92}\ [5.45\times10^4 < M_w < 2.68\times10^5] \\ EC_{2.5}: \quad & [\eta](cm^3/g) = 9.5\times10^{-4}M_w{}^{1.11}\ [6.34\times10^3 < M_w < 1.83\times10^4] \quad [\eta](cm^3/g) = 1.5\times10^{-2}M_w{}^{0.85}\ [5.29\times10^4 < M_w < 3.83\times10^5] \end{aligned} \tag{8}$$

The M_w dependencies of $[\eta]$ can be analyzed using the wormlike touched-bead model [32–34], as described in the SI. The solid lines in Fig. 8(a), (b) are the theoretical values calculated from the perturbed touched-bead model (Eqs. S5–S11) using molecular parameters determined from the M_w dependence of $\langle S^2\rangle_z^{1/2}$ and the bead diameters ($d_B = 1.8$ nm for $EC_{3.0}$ and 1.1 nm for $EC_{2.5}$) as an additional parameter. The theory consistently reproduces the experimental $[\eta]$ across the examined M_w range. The estimated d_B values are much larger than those obtained from SAXS ($d = 0.6$ nm), likely because SAXS ultimately measures the electron density difference between the polymer chain swollen by solvent and the surrounding solvent, thereby underestimating it. Furthermore, the d_B

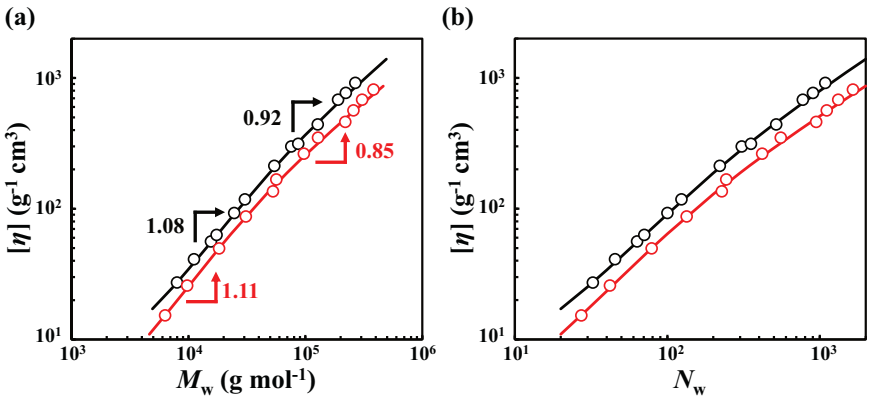

Fig. 8 **a** M_w dependence of $[\eta]$ for $EC_{3.0}$ (black circles) and $EC_{2.5}$ (red circles) in THF at 25 °C and **b** their N_w dependencies. The solid lines represent the theoretical curves for the perturbed KP touched-bead chain model with the parameters listed in Table 3

value for $EC_{2.5}$ is 1.6 times smaller than that for $EC_{3.0}$, indicating that $EC_{2.5}$ behaves as a hydrodynamically thinner polymer than $EC_{3.0}$ in THF at 25 °C, most likely because of desolvation around the remaining polar hydroxyl groups.

Next, the local conformation is described. The monomer contour length (l_M), which is related to the helical pitch and local conformation, is given by Eq. 9.

$$l_M = \frac{M_0}{M_L} \tag{9}$$

Here, M_0 is the molar mass of the repeating unit, as listed in Table 3. The l_M value was estimated to be 0.50 ± 0.03 nm for both $EC_{3.0}$ and $EC_{2.5}$, suggesting that the local conformation of the EC chain remains largely unaffected by x from 2.5 to 3.0. The l_M value obtained is almost equal to that (0.51–0.52 nm) of crystalline cellulose [35] and that (0.45–0.51 nm) of cellulose *tris*(alkyl carbamate) in THF [36] but considerably greater than that (0.13–0.19 nm) of cellulose in 1-butyl-3-methylimidazolium chloride ionic liquid [37] and that (0.33 nm) of α-1,4-linked amylose derivative [38], which assumes a gradual helical structure in solution.

Finally, the λ^{-1} value is discussed. The value increased from 16.5 to 23.1 nm as x increased from 2.5 to 3.0, likely due to increased steric hindrance from the greater number of ethyl groups. The λ^{-1} value for $EC_{3.0}$ obtained in this study is comparable to those of cellulose *tris*(phenylcarbamate) in THF (21 nm) [38] and 1-methyl-2-pyrrolidone (16 nm) [39], cellulose myristate (21 nm) [40], (cyanoethyl)(hydroxypropyl)cellulose (29 nm) [41], cellulose *tris*(ethylcarbamate) (17 nm) in THF [36], cellulose *tris*(*n*-butylcarbamate) (25 nm) in THF [36], and cellulose *tris*(*n*-octadecylcarbamate) (24 nm) in THF [36] but much greater than those of methylcellulose (11.6 nm) in water [42] and cellulose acetate (10 nm) in THF [43]. Compared with methylcellulose and cellulose acetate, which have substituents of similar size, $EC_{3.0}$ has considerably greater chain rigidity.

Conclusions

Molecular characterization of isolated ethylcellulose chains ($EC_{3.0}$ and $EC_{2.5}$) has been reported. The dimensional properties of ethylcellulose with a weight-averaged molar mass (M_w) ranging from 6.32×10^3 to 3.83×10^5 g mol^{-1} and a relatively narrow molar mass distribution ($M_w/M_n < 1.22$) were studied in THF at 25 °C using static light and small-angle X-ray scattering and the intrinsic viscosity. The z-averaged root-mean-squared radius of gyration and intrinsic viscosity for the isolated $EC_{3.0}$ and $EC_{2.5}$ chains were rationalized as functions of M_w, and their M_w dependencies were analyzed in terms of cylindrical wormlike chain and wormlike touched-bead models. The chain stiffness parameter (the Kuhn segment length, λ^{-1}), molar mass per unit contour length (M_L), and hydrodynamic bead diameter (d_B) were 23.1 nm, 491 g mol^{-1} nm^{-1}, and 1.8 nm for $EC_{3.0}$ and 16.5 nm, 467 g mol^{-1} nm^{-1}, and 1.1 nm for $EC_{2.5}$, respectively. Thus, $EC_{3.0}$ and $EC_{2.5}$ in THF at 25 °C behave as semiflexible chains with considerable stiffness. The monomer counter length (l_M) was estimated to be 0.50 nm for both $EC_{3.0}$ and $EC_{2.5}$, suggesting that the local conformation of the EC chain remains largely unaffected by x. The l_M value was almost equal to that of crystalline cellulose (0.51–0.52 nm) but considerably greater than that of α-1,4-linked amylose derivatives (0.33 nm). In contrast, the λ^{-1} and d_B values were significantly influenced by x, most likely due to increased steric hindrance along the cellulose backbone and the desolvation of residual polar hydroxyl groups.

Acknowledgements KF thanks Sumitomo Metal Mining Co., Ltd. for providing the opportunity for PhD research at Yamagata University.

Author contributions The manuscript was written through the contributions of all authors. All the authors have approved the final version of the manuscript.

Compliance with ethical standards

Conflict of interest The authors declare no competing interests.

Publisher's note Springer Nature remains neutral with regard to jurisdictional claims in published maps and institutional affiliations.

Open Access This article is licensed under a Creative Commons Attribution 4.0 International License, which permits use, sharing, adaptation, distribution and reproduction in any medium or format, as long as you give appropriate credit to the original author(s) and the source, provide a link to the Creative Commons licence, and indicate if changes were made. The images or other third party material in this article are included in the article's Creative Commons licence, unless indicated otherwise in a credit line to the material. If material is not included in the article's Creative Commons licence and your intended use is not permitted by statutory regulation or exceeds the permitted use, you will need to obtain permission directly from the copyright holder. To view a copy of this licence, visit http://creativecommons.org/licenses/by/4.0/.

References

1. Heinze T, El Seoud, OA, Koschella. Structure and properties of cellulose and its derivatives. springer series on polymer and composite materials. Springer International Publishing 2018. p. 39–172. https://doi.org/10.1007/978-3-319-73168-1_2.
2. Phair JW. Rheological analysis of concentrated zirconia pastes with ethyl cellulose for screen printing SOFC electrolyte films. J Am Ceram Soc. 2008;91:2130–7. https://doi.org/10.1111/j.1551-2916.2008.02443.x.
3. Sanson A, Gardini D, Montanari G, Galassi C, Roncari E. Key role of milling in the optimization of TiO_2 nanoinks. J Mater Res. 2006;21:1561–9. https://doi.org/10.1557/jmr.2006.0188.
4. Sugimura KI, Hirao K. Effect of a $BaTiO_3$ nanoparticle additive on the quality of thin-film Ni electrodes in MLCC. J Ceram Soc Jpn. 2009;117:1039–43. https://doi.org/10.2109/jcersj2.117.1039.
5. Lee S, Paik U, Yoon SM, Choi JY. Dispersant-ethyl cellulose binder interactions at the Ni particle-dihydroterpineol interface. J Am Ceram Soc. 2006;89:3050–5. https://doi.org/10.1111/j.1551-2916.2006.01192.x.
6. Jiang JS, Liang JE, Yi HL, Chen SH, Hua CC. Rheological fingerprints of time-evolving polymer-particle interaction and sol–gel transition in silver pastes. J Polym Res. 2015;22. https://doi.org/10.1007/s10965-015-0790-7.
7. Jiang JS, Liang JE, Yi HL, Chen SH, Hua CC. Performances of screen-printing silver thick films: rheology, morphology, mechanical and electronic properties. Mater Chem Phys. 2016;176:96–103. https://doi.org/10.1016/j.matchemphys.2016.03.032.
8. Murakami S, Ri K, Itoh T, Izu N, Shin W, Inukai K, Takahashi Y, Ando Y. Effects of ethyl cellulose polymers on rheological properties of (La, Sr)(Ti, Fe)$O_{3-\delta}$ terpineol pastes for screen printing. Ceram Int. 2014;40:1661–6. https://doi.org/10.1016/j.ceramint.2013.07.057.
9. Inukai K, Takahashi Y, Murakami S, Ri K, Shin W. Molecular weight dependence of ethyl cellulose adsorption behavior on (La, Sr)(Ti, Fe)$O_{3-\delta}$ particles in organic solvent pastes and their printing properties. Ceram Int. 2014;40:12319–25. https://doi.org/10.1016/j.ceramint.2014.04.077.
10. Inukai K, Takahashi Y, Ri K, Shin W. Rheological analysis of ceramic pastes with ethyl cellulose for screen-printing. Ceram Int. 2015;41:5959–66. https://doi.org/10.1016/j.ceramint.2015.01.032.
11. Sung JH, Lee JY, Kim S, Suh J, Kim J, Ahn KH, Lee SJ. Effect of particle size in Ni screen printing paste of incompatible polymer binders. J Mater Sci. 2010;45:2466–73. https://doi.org/10.1007/s10853-010-4218-9.
12. Tian Y, Mao C, Zhou X, Zhang H, Yin L, Ma S, Wang H. An optimization strategy for improving the aspect ratio of screen printing electronic paste based on rheological properties. Colloids Surf A Physicochem Eng Asp. 2024;697:134453. https://doi.org/10.1016/j.colsurfa.2024.134453.
13. Yi HL, Lai LJ, Jiang JS, Hua CC. Ethylcellulose colloids incubated in dilute solution. J Phys Chem B. 2017;121:638–48. https://doi.org/10.1021/acs.jpcb.6b09976.
14. Moore WR, Brown AM. Relationship between viscosity and molecular weight of ethyl cellulose. J Appl Chem. 1958;8:363–7. https://doi.org/10.1002/jctb.5010080604.
15. Scherer PC, Tanenbaum A, Levi DW. Molecular weight of ethyl cellulose. J Polym Sci. 1960;43:531–5. https://doi.org/10.1002/pol.1960.1204314223.
16. Meyerhoff G, Suetterlin N. Solution behavior of ethylcellulose in organic solvents. J Polym Sci Polym Symp. 1973;42:943–9. https://doi.org/10.1002/polc.5070420245.
17. Budgell DR. Liquid Crystalline Properties of Ethyl Cellulose. PhD Thesis in McGill University, 1989. https://escholarship.mcgill.ca/concern/theses/0v838131j.
18. Kikuchi M, Nakano R, Jinbo Y, Saito Y, Ohno S, Togashi D, Enomoto K, Narumi A, Haba O, Kawaguchi S. Graft density dependence of main chain stiffness in molecular rod brushes. Macromolecules. 2015;48:5878–86. https://doi.org/10.1021/acs.macromol.5b01010.
19. Suzuki Y, Watanabe T, Kosugi H, Ueda K, Kikuchi M, Narumi A, Kawaguchi S. Chain conformation of poly(D-Lactide) in tetrahydrofuran by static light scattering, small-angle X-ray scattering, and intrinsic viscosity. Macromolecules. 2020;53:1604–12. https://doi.org/10.1021/acs.macromol.9b02532.
20. Matsumoto Y, Kikuchi M, Ueda K, Enomoto K, Narumi A, Kawaguchi S. Highly reliable determination of the interdetector delay volume in SEC-MALS for precise characterization of macromolecules having narrow and broad molar mass distributions. Polym J. 2023;55:239–51. https://doi.org/10.1038/s41428-022-00744-7.
21. Suzuki Y, Watanabe T, Kosugi H, Ueda K, Kikuchi M, Narumi A, Kawaguchi S. Dilute solution properties of poly(D,L-Lactide) by static light scattering, SAXS, and intrinsic viscosity. Polym J. 2020;52:387–96. https://doi.org/10.1038/s41428-019-0293-1.
22. Streeter DJ, Boyer RF. Solution viscosity and partial specific volume of polystyrene. effect of solvent type and concentration. Ind Eng Chem. 1951;43:1790–7. https://doi.org/10.1021/ie50500a032.
23. Itou T, Chikiri H, Teramoto A, Aharoni SM. Wormlike chain parameters of poly(Hexyl Isocyanate) in dilute solution. Polym J. 1988;20:143–51. https://doi.org/10.1295/polymj.20.143.
24. Terao K, Fujii T, Tsuda M, Kitamura S, Norisuye T. Solution properties of amylose tris(Phenylcarbamate): local conformation and chain stiffness in 1,4-dioxane and 2-ethoxyethanol. Polym J. 2009;41:201–7. https://doi.org/10.1295/polymj.PJ2008233.
25. Konishi T, Yoshizaki T, Saito T, Einaga Y, Yamakawa H. Mean-square radius of gyration of oligo- and polystyrenes in dilute solutions. Macromolecules. 1990;23:290–7. https://doi.org/10.1021/ma00203a050.
26. Benoit H, Doty P. Light scattering from non-Gaussian chains. J Phys Chem. 1953;57:958–63. https://doi.org/10.1021/j150510a025.
27. Murakami H, Norisuye T, Fujita H. Dimensional and hydrodynamic properties of poly(hexyl isocyanate) in hexane. Macromolecules. 1980;13:345–52. https://doi.org/10.1021/ma60074a026.
28. Domb C, Barrett AJ. Universality approach to the expansion factor of a polymer chain. Polymer. 1976;17:179–84. https://doi.org/10.1016/0032-3861(76)90096-3.
29. Yamakawa H, Stockmayer WH. Statistical mechanics of wormlike chains. ii. excluded volume effects. J Chem Phys. 1972;57:2843–54. https://doi.org/10.1063/1.1678675.

30. Yamakawa H, Shimada J. Stiffness and excluded-volume effects in polymer chains. J Chem Phys. 1985;83:2607–11. https://doi.org/10.1063/1.449254.
31. Shimada J, Yamakawa H. Statistical mechanics of helical wormlike chains. XV. excluded-volume effects. J Chem Phys. 1986;85:591–600. https://doi.org/10.1063/1.451853.
32. Yoshizaki T, Nitta I, Yamakawa H. Transport coefficients of helical wormlike chains. 4. Intrinsic viscosity of the touched-bead model. Macromolecules. 1988;21:165–71. https://doi.org/10.1021/ma00179a033.
33. Kirkwood JG, Riseman J. The intrinsic viscosities and diffusion constants of flexible macromolecules in solution. J Chem Phys. 1948;16:565–73. https://doi.org/10.1063/1.1746947.
34. Barrett AJ. Intrinsic viscosity and friction coefficients for an excluded volume polymer in the Kirkwood approximations. Macromolecules. 1984;17:1566–72. https://doi.org/10.1021/ma00138a024.
35. Nishiyama Y, Langan P, Chanzy H. Crystal structure and hydrogen-bonding system in cellulose Iβ from synchrotron X-Ray and neutron fiber diffraction. J Am Chem Soc. 2002;124:9074–82. https://doi.org/10.1021/ja0257319.
36. Jiang XY, Ryoki A, Terao K. Dimensional and hydrodynamic properties of cellulose tris(alkylcarbamate)s in solution: side chain dependent conformation in tetrahydrofuran. Polymer. 2017;112:152–8. https://doi.org/10.1016/j.polymer.2017.02.012.
37. Jiang X, Kitamura S, Sato T, Terao K. Chain dimensions and stiffness of cellulosic and amylosic chains in an ionic liquid: cellulose, amylose, and an amylose carbamate in BmimCl. Macromolecules. 2017;50:3979–84. https://doi.org/10.1021/acs.macromol.7b00389.
38. Kasabo F, Kanematsu T, Nakagawa T, Sato T, Teramoto A. Solution properties of cellulose tris(Phenyl Carbamate). 1. Characterization of the conformation and intermolecular interaction. Macromolecules. 2000;33:2748–56. https://doi.org/10.1021/ma991443u.
39. Norisuye T, Tsuboi A, Sato T, Teramoto A. Solution properties of cellulose tris(3,5-dimethyl-phenylcarbamate). Macromol Symp. 1997;120:65–76. https://doi.org/10.1002/masy.19971200109.
40. Bushin SV, Khripunov AK, Bezrukova MA, Astapenko EP. Hydrodynamic and conformational properties of cellulose myristate molecules in solution. Polym Sci A. 2007;49:71–6. https://doi.org/10.1134/S0965545X07010105.
41. Mays JW. Solution properties and chain stiffness of (cyanoethyl) (hydroxypropyl) cellulose. Macromolecules. 1988;21:3179–83. https://doi.org/10.1021/ma00189a009.
42. Bodvik R, Dedinaite A, Karlson L, Bergström M, Bäverbäck P, Pedersen JS, Edwards K, Karlsson G, Varga I, Claesson PM. Aggregation and network formation of aqueous methylcellulose and hydroxypropylmethylcellulose solutions. Colloids Surf A Physicochem Eng Asp. 2010;354:162–71. https://doi.org/10.1016/j.colsurfa.2009.09.040.
43. Saito M. Wormlike chain parameters of cellulose and cellulose derivatives. Polym J. 1983;15:213–23. https://doi.org/10.1295/polymj.15.213.